16th World Conference on Earthquake Engineering, 16WCEE 2017

Santiago Chile, January 9th to 13th, 2017

Paper N° 2855

Registration Code: S-Z1464597232

Strong ground motion simulation of the 2005 Central Chiba intraslab earthquake with the pseudo point-source model

Y. Nagasaka[(1)], A. Nozu[(2)]

[(1)] *Researcher of the Engineering Seismology Group, Port and Airport Research Institute, nagasaka-y@pari.go.jp*
[(2)] *Director of the Earthquake Disaster Prevention Engineering Division, Port and Airport Research Institute, nozu@pari.go.jp*
…

Abstract

Validated strong ground motion simulation methods are important for an earthquake-resistant design of structures. However, in the technical standards for ports in Japan, limited methods are available to evaluate shaking from intraslab earthquakes, which occur inside subducting plates. In this study, strong ground motion simulations that use the pseudo point-source model were conducted on the July 23, 2005 Central Chiba intraslab earthquake, which occurred under the Tokyo metropolitan area. The purpose is to develop a suitable strong ground motion estimation method for intraslab earthquakes. Results are analyzed to identify the applicability and understand the limitations of the model. The strong ground motion simulation showed a generally good agreement with observed records. However, underestimation of observed ground motions was found at several stations west of the epicenter. One of the possible causes is the rupture directivity effect, which the current version of the pseudo point-source model does not consider. The rupture process estimated by waveform inversion indicated that the rupture propagated toward the surface. This rupture can cause forward rupture directivity effect at the underestimated stations. We then attempted to introduce a corner frequency model that expressed the rupture directivity effect of unilateral rupture. The modelled corner frequencies do not match the observed corner frequencies. Although considering the directivity effect was unnecessary for the 2005 Central Chiba intraslab earthquake, we continued to investigate the applicability of the model. Variation in the site amplification factors is discussed as another potential cause of the underestimation. At the underestimated stations, the site amplification factors of the intraslab earthquakes that occurred near the 2005 Central Chiba earthquake were found to be larger than those of the earthquakes that occurred at various locations. The results of the simulation were improved with the use of corrected site amplification factors for intraslab earthquakes.

Keywords: strong ground motion simulation, pseudo point-source model, intraslab earthquake

1. Introduction

The validation of strong ground motion simulation methods is important for the satisfactory estimation of site-specific strong ground motions. Underestimated strong ground motions can cause unexpected and extensive damages to structures, especially in large cities, such as the Tokyo metropolitan area. The Central Disaster Management Council of Japan reported that a M_w7.3 intraslab earthquake can occur south of the Tokyo Metropolitan area, so measures should be taken for disaster prevention and mitigation [1]. In the technical standards for Japanese ports, however, limited methods are available to estimate strong ground motions for intraslab earthquakes.

In this study, a strong ground motion simulation of the July 23, 2005 Central Chiba earthquake is conducted with the pseudo point-source model to establish a method of strong ground motion simulation for intraslab earthquakes [2]. The results are compared with the observed records and analyzed, with a focus on the causes of the underestimation.

The July 23, 2005 Central Chiba earthquake (M_w5.9) is the largest intraslab earthquake to have occurred south of the Tokyo Metropolitan area since the establishment of nationwide dense strong-motion networks. This earthquake is therefore suitable for the purpose of our study. Because only one earthquake is examined in this study, a general validation of the applicability of the pseudo point-source model is not achieved. However, the applicability or limitations of the source model can be clarified with the accumulation of studies on individual earthquakes, and the current study is the first step toward such a goal.

The pseudo point-source model, proposed by Nozu, is a simplified source model for strong ground motion simulation (2012) [2]. The source model can explain the observed records as well as the characterized source models for the 2011 Tohoku earthquake [2]. The source model can also be applied to intraslab earthquakes. Nevertheless, the pseudo point-source model is a relatively new source model, so several limitations may need to be addressed.

2. Strong ground motion simulation with the pseudo point-source model

2.1 Pseudo point-source model

In the pseudo point-source model, the spatio-temporal distribution of the slip is not considered explicitly. By contrast, characterized source models usually assume rectangular sub-events that are divided into smaller grids. Despite its simplicity, the source model can well reproduce observed records [2].

Waveforms are synthesized with the inverse Fourier transform of the evaluated frequency spectra $A(f)$. $A(f)$ is calculated by multiplying the contribution of source $S(f)$, path $P(f)$, site amplification $G(f)$, and phase $O(f)/|O(f)|_p$, as shown in Eq. (1).

$$A(f) = S(f)P(f)G(f)\frac{O(f)}{|O(f)|_p} \ . \tag{1}$$

$S(f)$ and $P(f)$ are calculated with Eq. (2) and Eq. (3), respectively [3].

$$S(f) = R_{\theta\phi} \cdot PRTITN \cdot FS \cdot \frac{M}{4\pi\rho V_S^3} \cdot \frac{(2\pi f)^2}{1+(f/f_c)^2} \ , \tag{2}$$

$$P(f) = \frac{1}{r} exp\left(-\frac{\pi r f}{QVs}\right), \tag{3}$$

where $R_{\theta\phi}$ is the radiation coefficient, $PRTITN$ is the coefficient to divide the seismic energy into two horizontal directions, FS is the amplification factor by the free surface (=2.0), M is the seismic moment,

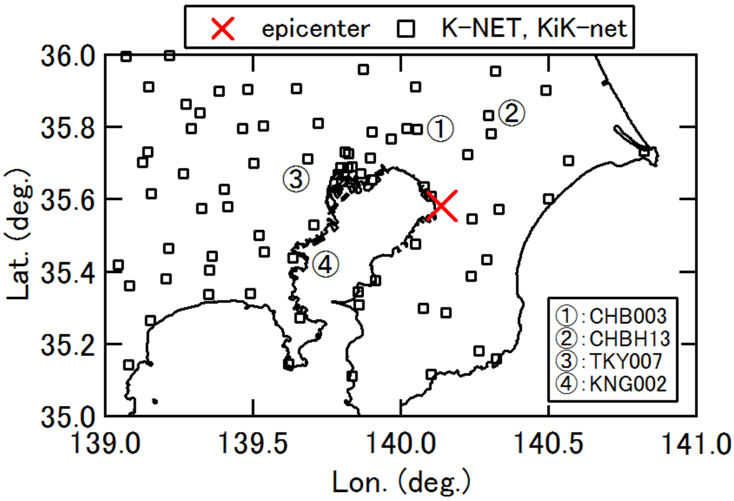

Fig. 1 Epicenter and target stations of the strong ground motion simulation

ρ and V_S are the density and S wave velocity around the hypocenter, respectively, f is the frequency, f_c is the corner frequency, r is the hypocentral distance to the target station, and Q is the quality factor.

For $G(f)$, an empirical model is commonly used. $O(f)$ is the Fourier transform of a previous small earthquake record at the target station. $|O(f)|_p$ is the absolute value of $O(f)$ to which a Parzen window of 0.05 Hz bandwidth is applied. Thus, $O(f)/|O(f)|_p$ is a complex spectrum whose absolute value is almost 1. In the phase characteristics, we assume that the selected small earthquake has the same phase characteristics as the target earthquake.

As shown in Eq. (1), a simple source spectrum that follows the omega square model [4] is given for each sub-event. Size and rupture propagation parameters are not used. The size of the source is considered by a corner frequency that is inversely proportional to the size of a sub-event. However, the effect of rupture propagation is not explicitly considered.

2.2 Target stations and parameters

The epicenter and the target stations are shown in Fig. 1. In this study, all the K-NET and KiK-net stations [5, 6] within the area shown in Fig. 1 are used. Empirical site amplification factors $G(f)$ were already evaluated for the K-NET and KiK-net stations by Nozu and Nagao (2005) [7].

Table 1 shows the parameters determined. Only one sub-event for the earthquake and most parameters are consistent with those in previous studies. Corner frequency is determined by trial and error.

Table 1 – Parameters of the strong ground motion simulation

Target earthquake[1]	July 23, 2005 16:34 (JST) Central Chiba earthquake (M_w5.9)
Epicenter[2]	35.5817°, 140.1385°
Depth[3]	68 km
Strike, dip, rake[4]	8°, 72°, 93°
Seismic moment[4]	9.39×10^{17} Nm
Density around the hypocenter[5]	3.4 g/cm^3
S wave velocity around the hypocenter[5]	4.6 km/s
Q[6]	$100\times f^{0.7}$
Radiation coefficient	Average value (=0.63)
Corner frequency	0.75 Hz
Small earthquake for phase characteristics[1]	August 6, 2004 03:23 (JST) Central Chiba earthquake (M_w4.7)

1: The date is from the Japan Meteorological Agency. The M_w is from F-net [6].
2: From the Japan Meteorological Agency
3: From F-net [6]
4: From Hayakawa (2014) [8]
5: From The Headquarters for Earthquake Research Promotion (2012) [9]
6: From the Central Disaster Management Council (2001) [10]

3. Results

In this section, the results of the strong ground motion simulation are compared with observed records.

3.1 Velocity time history and Fourier spectrum

The synthesized and observed velocity time histories are compared in Fig. 2. A bandpass filter of 0.2 Hz to 2 Hz is applied. The result shows a generally good agreement with the observed records in terms of amplitude and phase characteristics.

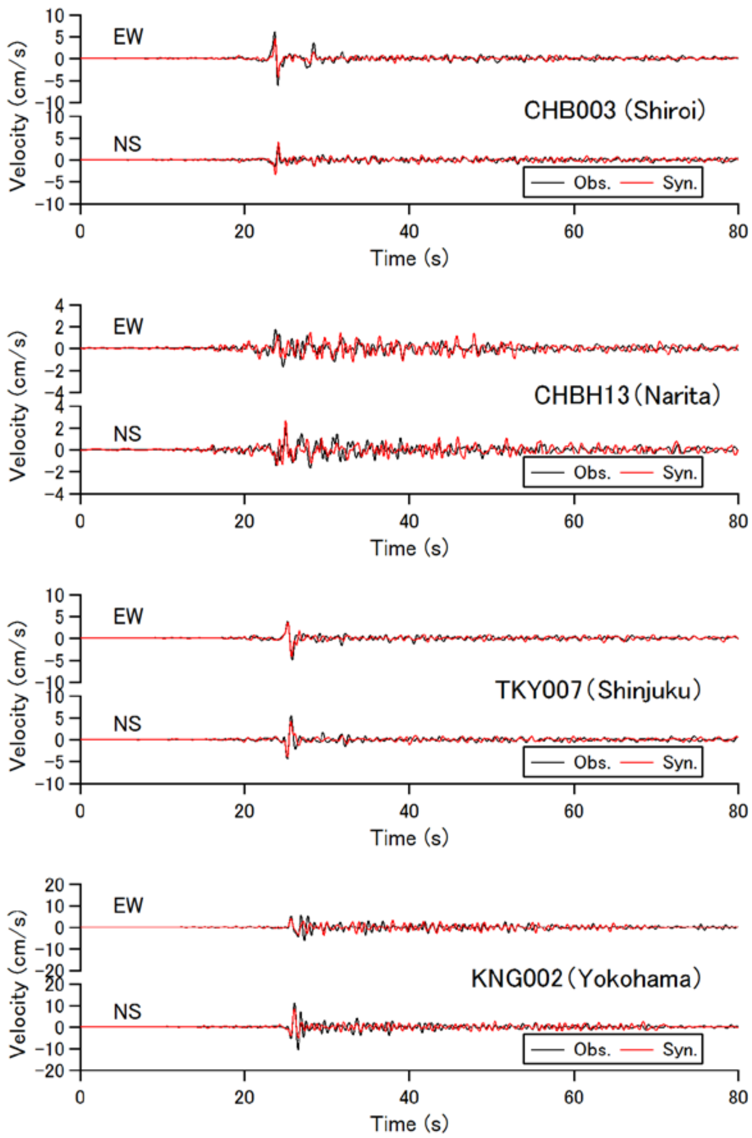

Fig. 2 – Observed and simulated velocity time histories (station locations are shown in Fig. 1)

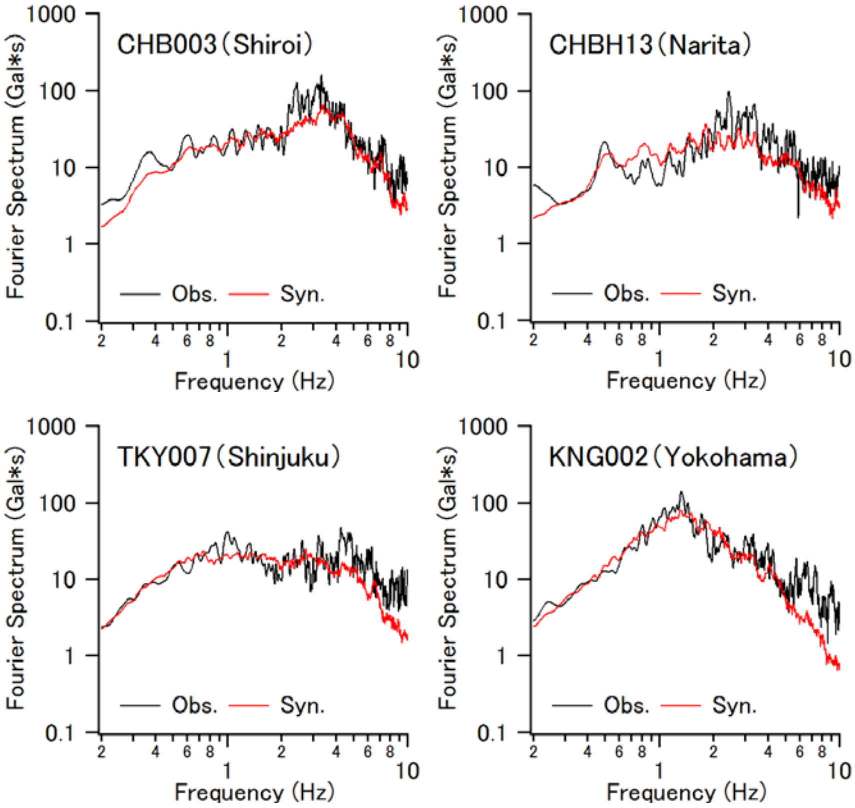

Fig. 3 – Observed and simulated acceleration Fourier spectrum (station locations are shown in Fig. 1)

The synthesized and observed acceleration Fourier spectra are compared in Fig. 3. The synthesized spectra reproduce well the characteristics of the observed records, such as peak frequency and low frequency level.

3.2 PSI ratio

The power spectral intensity (PSI) ratio is calculated to identify quantitatively the results at all target stations. PSI is an index calculated from velocity time histories by Eq. (4), where *Vel*(t) is the horizontal component of velocity time history. PSI has good correlation with the displacement of quay walls because of strong ground motions [11]. Fig. 4 shows the distribution of the PSI ratio (synthesis/observation).

$$PSI = \sqrt{\int Vel(t)^2 \, dt} \tag{4}$$

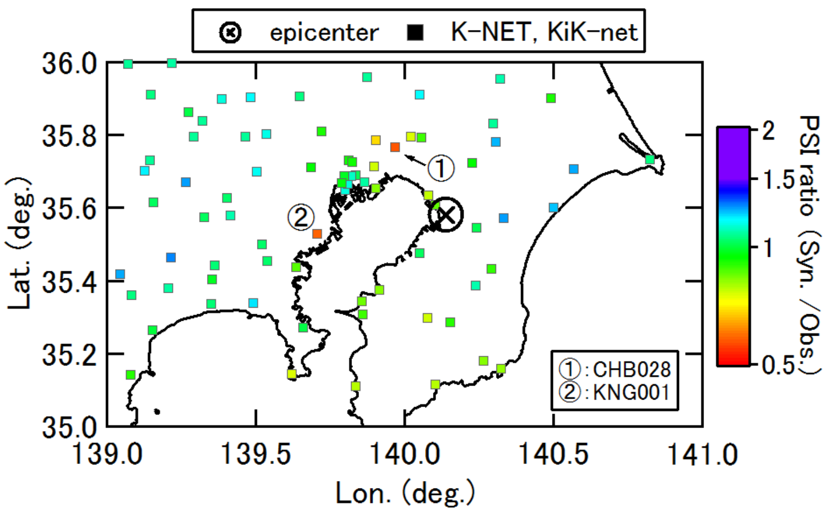

Fig. 4 – Distribution of the PSI ratio

In Fig. 4, the PSI ratio is close to 1.0 at many stations. However, some stations in the west and north of Tokyo Bay, such as CHB028 and KNG001, were significantly underestimated (red color). The results at CHB028 and KNG001 are shown in Fig. 5. We can see that the amplitude in the EW direction is particularly underestimated at both stations. The Fourier spectrum is also underestimated. Underestimation is not desirable in strong ground motion simulation for an earthquake-resistant design because if underestimated motions are used in the structural design, structures can suffer unexpected damage arising from strong motions. Investigating the causes of underestimation is thus important. Two possible causes are examined in this study. One is rupture directivity, which is not considered in the pseudo point-source model. If the rupture propagates to the up-dip direction, i.e., to the surface, strong motions are coherently superposed according to the rupture progression. As a result, strong motions on the ground will be larger than those from a point-source model that does not consider the finiteness of the fault. Another possible cause is the inaccuracy of site amplification factors. Depending on the incident angle of seismic waves into the sedimentary layer or the heterogeneity of the media, site amplification factors can vary. The site amplification factors we used in the simulation were average values used for not only intraslab earthquakes. If we use only intraslab earthquakes that occurred near the target earthquake, the site amplification factors can be different.

4. Analyses

In this section, we discuss two possible causes of the underestimation mentioned in Section 3, namely rupture directivity and inaccuracy of site amplification factors.

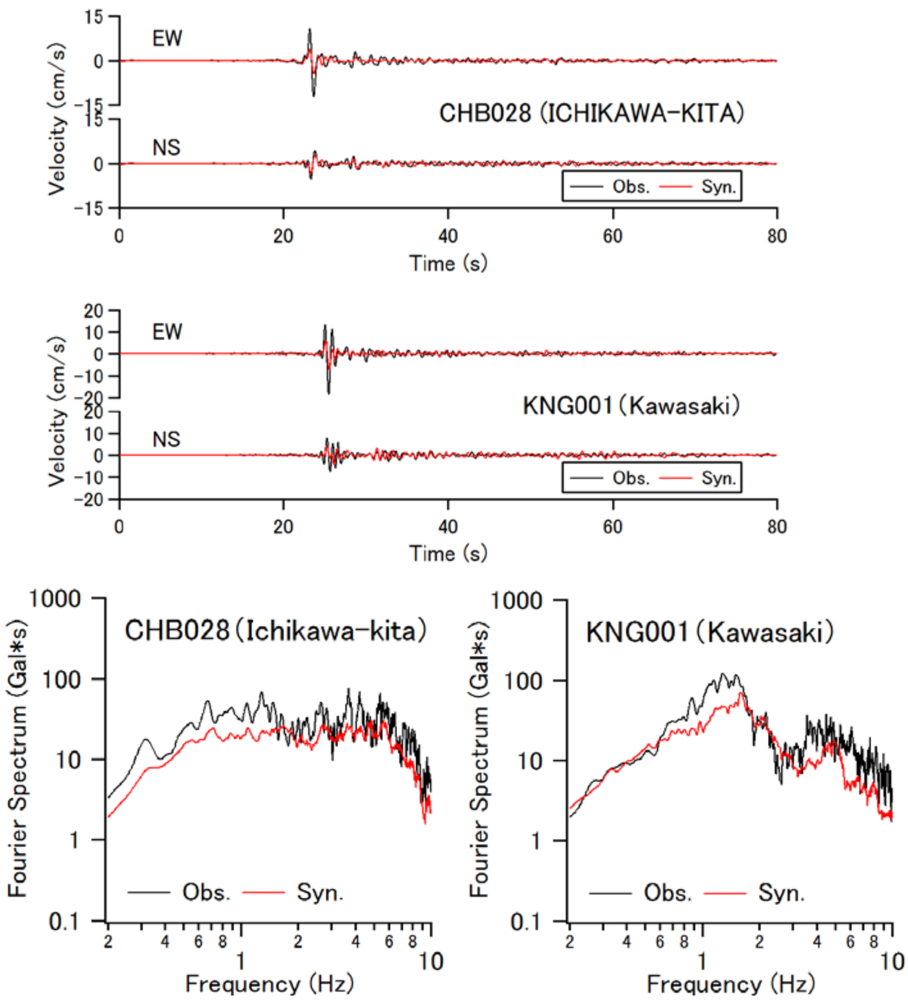

Fig. 5 – Observed and simulated velocity time histories and Fourier spectrum at the underestimated stations

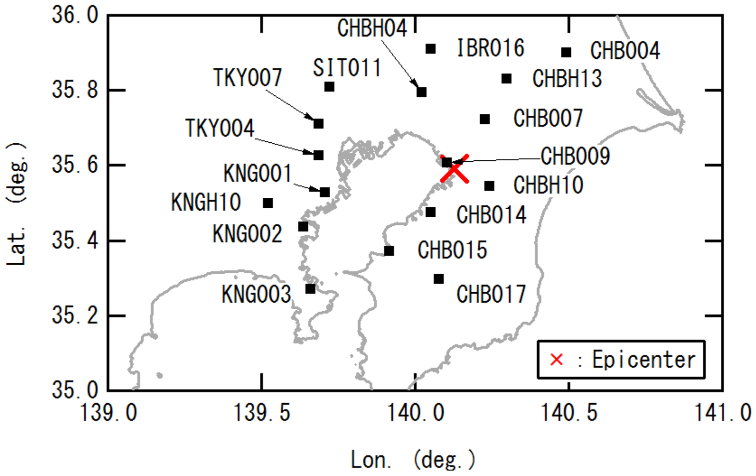

Fig. 6 – Stations used in the waveform inversion

4.1 Rupture process by waveform inversion

Waveform inversion using empirical Green's function [12, 13] was conducted to estimate the rupture process. The earthquake used in the empirical Green's function is the same one used in the phase characteristics in Section 2 (see Table 1). The stations used are shown in Fig. 6. Velocity time histories of 0.2 Hz to 1.5 Hz are used for the inversion. The parameters are determined to be consistent with those in Table 1. The additional parameters required are the fault length and width (8 and 10 km, respectively), as well as the rise time (=2.5 s). The fault plane is divided into 1 km × 1 km grids, and the seismic moment is estimated every 0.1 s at each grid. The rupture front is assumed to spread concentrically from the hypocenter with a velocity of 3.6 km/s.

The estimated slip distribution is shown in Fig. 7. The maximum slip was 0.5 m. Fig. 7 indicates that the rupture propagated almost unilaterally to the up-dip direction. This rupture means that forward rupture directivity can appear on the ground around the north of Tokyo Bay. The results could be improved by considering the rupture directivity effect in the pseudo point-source model.

4.2 Corner frequency model

Incorporating a complex model into the pseudo point-source model to include the rupture directivity effect is undesirable because simplicity is an important characteristic of the model. We considered introducing a corner frequency model, as shown in Eq. (5). If the rupture propagated in the up-dip direction unilaterally, according to the Haskell model, the effect of rupture propagation is expressed by a change in corner frequency:

$$f_c = \frac{V_r}{\pi L} \frac{1}{1 - \frac{V_r}{V_s} \cos\varphi}, \tag{5}$$

where V_r is the rupture velocity, L is the rupture length, and φ is the angle between the direction of rupture progression and the direction to the target station from the source. Eq. (5) means that the corner frequency is highest in the direction of the rupture propagation (φ=0) and smallest in the opposite direction (φ=π). By introducing this corner frequency model, we can consider the rupture directivity effect approximately without assuming finite sources.

In Fig. 8, the modelled corner frequency is compared with the corner frequencies by which the Fourier spectrum error in Eq. (6) is minimized, so we can identify the applicability of the corner frequency model by Eq. (5).

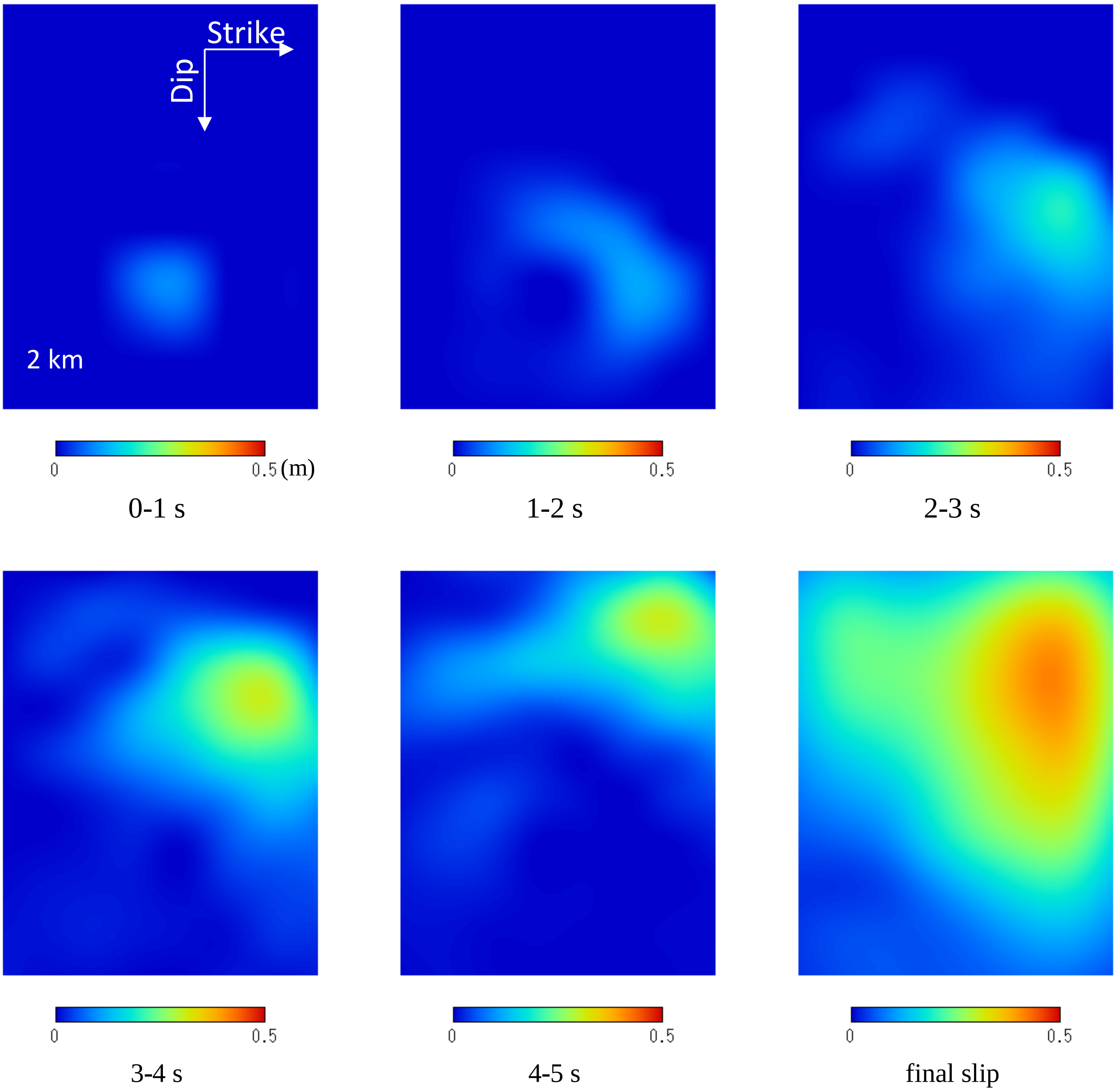

Fig. 7 – Estimated slip distribution every 1 s and the final slip

$$Fourier\ spectrum\ error = \int_{f=0.2Hz}^{f=2Hz} \left(\log_{10} FS_{syn} - \log_{10} FS_{obs}\right)^2 d\left(\log_{10} f\right), \tag{6}$$

where FS_{syn} and FS_{obs} are the synthesized and observed acceleration Fourier spectra, respectively. In Fig. 8 (a), the parameters of Eq. (5) are determined to be consistent with the waveform inversion in Section 4.1 and the rupture is assumed to propagate in the up-dip direction. Fig. 8 (a) shows that the corner frequency model by Eq. (5) does not explain well the corner frequencies determined with Eq. (6); it does not seem to be clearly dependent on φ, and a uniform value of 0.75 Hz (in Table 1) seems to match better. This result indicates that the rupture directivity effect is not observed in the records, contrary to the result of the waveform inversion. This inconsistency can be because the rupture process estimated in Fig. 7 is not completely unilateral but is a combination of unilateral and circular ruptures. In circular rupture, the corner frequency is independent of φ, so the resulting dependency of the corner frequency on φ is weaker when the rupture is a combination of unilateral and circular ruptures.

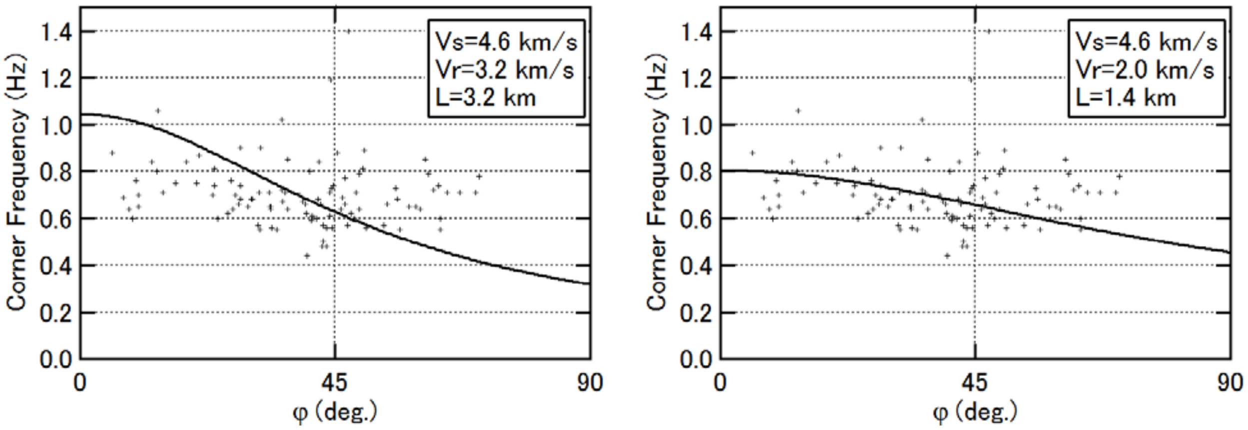

(a) (b)

Fig. 8 – Comparison of corner frequencies. Solid line: modelled corner frequency by Eq. (5). Marker: corner frequencies determined so that the Fourier spectrum error by Eq. (6) is minimized for each station.

a: The parameters in Eq. (5) are consistent with the result of the waveform inversion, b: The parameters in Eq. (5) are adjusted to explain the corner frequencies, which minimizes the Fourier spectrum error by Eq. (6).

We then adjusted the parameters in Eq. (5) so that the total square root error between the model by Eq. (5) and the markers in Fig. 8 (a) is minimized. The revised corner frequency model and parameters are shown in Fig. 8 (b). An important issue to note here is that the parameters in Fig. 8 (b) do not have physical meaning and are inconsistent with the waveform inversion. The parameters are distorted to explain the observed records, including not only the effect of rupture propagation but also the non-unilateral portion of the rupture. Fig. 8 (b) shows that adjustment of the parameters made the corner frequency model by Eq. (5) close to the constant value.

In the 2005 Central Chiba earthquake, the corner frequency model by Eq. (5) does not improve the pseudo point-source model. This result means that the effect of rupture propagation was unclear for the intraslab earthquake. However, this is the result of one intraslab earthquake, and there are shallow crustal earthquakes whose rupture directivity effect was clearly observed. We will investigate the applicability of the corner frequency model by using other earthquakes.

4.3 Uncertainty in the site amplification factor

Another possible source of underestimation at particular stations is variations in site amplification factors. We used the empirical site amplification factor from Nozu and Nagao (2005) in the simulation. This factor was evaluated with the spectral inversion method, in which the estimated source and path spectra were divided from the observed Fourier spectrum with the use of many small and middle earthquake records. Depending on the incident angle of seismic waves, amplification in the sedimentary layer can vary. This variation is considered because of the 3D effect or heterogeneity in the small scale. Thus, depending on the location of the hypocenter and other factors, site amplification factors can be different.

To investigate the differences in site amplification factors by hypocenter location, we selected KNG001 and CHB028 as the underestimated stations and calculated the spectral ratio with a nearby station (KNG001/KNG002 and CHB028/CHB003); we used nine earthquakes that occurred near the 2005 Central Chiba earthquake (Fig. 9). KNG002 and CHB003 are not underestimated, although they are near the underestimated stations. When two stations are close to each other relative to the hypocentral distance, the source and path effect can be considered the same. In this case, the distance between KNG001 and KNG002 is 12 km, and that between CHB028 and CHB003 is 9 km, whereas the hypocenter depth is 68 km. Thus, the spectral ratio approximately represents the difference between the site amplification factors of the two stations. Under this assumption, the calculated spectral ratio of an observed intraslab earthquake record is compared with the ratio of the site amplification factors by Nozu and Nagao (2005). The result is shown in Fig. 10 (a). Fig. 10 (a) depicts that variation remains despite the use of earthquakes that occurred in the same region (gray lines). However, the average ratio of intraslab earthquakes (green line) clearly exceeds the ratio of the site amplification factors (black line). This result means that intraslab earthquakes cause greater

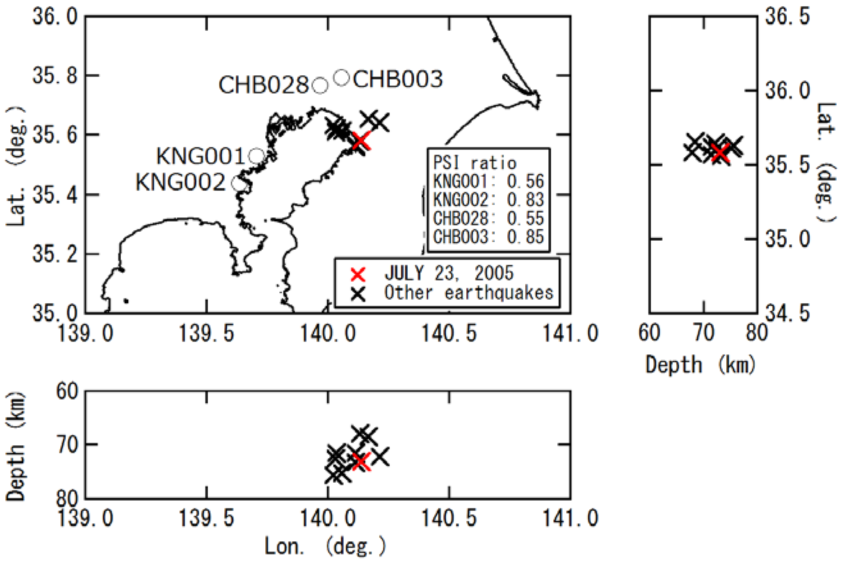

Fig. 9 – Hypocenter locations used to estimate the site amplification factors for intraslab earthquakes at KNG001 and CHB028

amplification at KNG001 and CHB028 than the average site amplification by Nozu and Nagao (2005). By multiplying this empirical observed spectral ratio of intraslab earthquakes (green line in Fig. 10 a) to the synthesized spectrum at KNG002 and CHB003 (red line in Fig. 3), we can obtain the corrected synthesized spectra for intraslab earthquakes at KNG001 and CHB028. In Fig. 10 (b), the corrected spectrum (blue line) is added to Fig. 5. The blue line matches better than the original red line. With the correction, the PSI ratio is improved from 0.56 to 0.70 at KNG001 and from 0.55 to 0.87 at CHB028.

5. Conclusion

We developed a pseudo point-source model for the July 23, 2005 Central Chiba earthquake and conducted strong ground motion simulations to check the applicability of the source model for the intraslab earthquake. The results of the simulation showed a generally good agreement with the observed records. However, motions were underestimated at stations to the west of the epicenter, such as KNG001 and CHB028. As the possible reasons for the underestimation, rupture directivity and uncertainty in the site amplification factors were investigated. The result of waveform inversion suggested that rupture directivity effect can amplify the strong motions at underestimated stations, but this effect was not considered in the pseudo point-source model. We then attempted to incorporate a corner frequency model into the pseudo point-source model so that the rupture directivity effect is represented. We found that the corner frequency model did not improve the results, indicating that directivity was not clearly seen in the observed records. This result means that directivity was unnecessary for the intraslab earthquake. However, we need to investigate other earthquakes in which directivity was clearly observed. As for the uncertainty in site amplification factors, dependency on the location of the hypocenter was examined. The amplifications in the sedimentary layer by intraslab earthquakes at KNG001 and CHB028, where underestimation was observed, were found to be greater than the amplifications estimated by Nozu and Nagao (2005), in which not only intraslab earthquakes were used. The simulated results were improved with the use of corrected site amplification factors for intraslab earthquakes. Reevaluating site amplification factors is desirable in simulating intraslab earthquakes, but further validation is necessary.

6. References

[1] Central Disaster Management Council (2013): http://www.bousai.go.jp/jishin/syuto/taisaku_wg/pdf/syuto_wg_report.pdf. In Japanese.

[2] Nozu A (2012): A simplified source model to explain strong ground motions from a huge subduction earthquake -Simulation of strong ground motions for the 2011 off the Pacific Coast of Tohoku earthquake with a pseudo point-source model-. *Zisin 2*, 65, 45-67.

[3] Boore D.M. (1983): Stochastic simulation of high-frequency ground motions based on seismological models of the radiated spectra. *Bulletin of the Seismological Society of America*, 73, 1865-1894.

[4] Aki K, Richards PG (2002): Quantitative Seismology. Second Edition, University Science Books.

[5] Aoi S, Kunugi T, Fujiwara H (2004): Strong-motion seismograph network operated by NIED: K-NET and KiK-net. *Journal of Japan Association for Earthquake Engineering*, 4, 65-74.

[6] Okada Y, Kasahara K, Hori S, Obara K, Sekiguchi S, Fujiwara H, Yamamoto A (2004): Recent progress of seismic observation networks in Japan -Hi-net, F-net, K-NET and KiK-net-. *Earth Planets Space*, 56, xv-xxviii.

[7] Nozu A, Nagao T (2005): Site amplification factors for strong-motion sites in Japan based on spectral inversion technique. *Technical Note of the Port and Airport Research Institute*, No.1112, in Japanese.

[8] Hayakawa T (2014): Point source parameters of the 23 July 2005 Mj6.0 Central Chiba earthquake. *The 14th Japan Earthquake Engineering Symposium*, GO15-Fri-7, in Japanese.

[9] The Headquarters for Earthquake Research Promotion (2012): http://www.jishin.go.jp/main/chousa/12_choshuki/choshuki2012_a2.pdf. in Japanese.

[10] Central Disaster Management Council (2001): http://www.bousai.go.jp/jishin/tokai/senmon/8/pdf/siryou.pdf. in Japanese.

[11] Nozu A, Iai S (2001): A ground motion index suitable for real time damage assessment of quay walls. *Proceedings of the 28th Regional Meeting in Kanto*, 18-19, in Japanese.

[12] Hartzell SH (1978): Earthquake aftershock as Green's functions. *Geophysical Research Letters*, 5, 1-4.

[13] Hartzell SH and Heaton TH (1983): Inversion of strong ground motion and teleseismic waveform data for the fault rupture history of the 1979 Imperial valley, California, earthquake. *Bulletin of the Seismological Society of America*, 73, 1553-1583.